Mustapha ZAOUIA[1], Arezki FEKIK[2], Abderrezak BADJI[1], Nacereddine BENAMROUCHE[1]

LATAGE Laboratory, Mouloud Mammeri University of Tizi-Ouzou, Algeria (1), Akli Mohand Oulhadj University of Bouira , Algeria (2)

doi:10.15199/48.2021.01.03

A thermal model for induction motor analysis under faulty operating conditions by using finite element method

Abstract. *The aim of this work is to present an electromagnetic-thermal model of a Three-phase squirrel cage induction motor taking into account faulty operating conditions. The model is based on the resolution of the stationary electromagnetic equation, in terms of magnetic vector potential (MVP) coupled to the thermal equations using finite element method (FEM). The coupling of electromagnetic and thermal phenomenon is ensured through the power density. The considered faults are principally the ones due to the open-circuit of a phase and broken rotor bars. We will study the influence of the different considered faults on the magnetic flux with harmonic spectrum analysis and the temperature in strategic regions of the motor.*

Streszczenie. *Przedstawiono elektromagnetyczny/termiczny model trójfazowego klatkowego silnika indukcyjnego z uwzględnieniem jego uszkodzenia. Do modelowania wykorzystano metodę elementu skończonego. Analizowano wpływ różnych uszkodzeń na pracę silnika. (**Model termiczny silnika indukcyjnego uwzględniający jego uszkodzenia i wykorzystujący metodę element€ skończonego**)*

Keywords: Thermal modeling, Induction Motor, Finite Element Method, Broken bars and open circuits.
Słowa kluczowe: diagnostyka, silnik indukcyjkny, model termiczny.

Introduction

The induction motors have known an accelerated growth in the last decades. Indeed, they are the most used in industrial domain and also in domestic application. Induction motor especially squirrel cage motor is very simple and it is almost unbreakable. Its cost is low; it is highly reliable and rugged. Moreover, squirrel cage motors have a very high efficiency, but their main disadvantage is that they are subject to different types of faults. In industry, squirrel-cage motors are often exposed to hostile environment or subject to manufacturing defects leading to failure in the industrial process. To avoid this, maintenance specialists integrate online monitoring systems for all the relevant information concerning the state of the motor. Reliable functioning of induction motors is related to minimizing machine downtime and maintaining high performance, which contributes to scrap-free production and overall sustainability in manufacturing. For all these reasons, the diagnosis and detection of failures in squirrel cage induction motors become necessary in order to avoid catastrophic accidents [1, 2, 3].

The faults may be broken bar fault, bearing fault, rotor mass unbalance fault, bowed rotor fault, stator winding fault, single phasing fault, and crawling. The effects of these faults include unbalanced stator currents and voltages, oscillations in torque, reduction in efficiency, overheating, and excessive vibrations. Moreover, these faults can increase the magnitude of certain harmonic components of currents and voltages [4, 5, 6, 7].

In recent years, there has been significant progress in the field of the fault analysis and maintenance of induction machines, with the extension of computer techniques, and control techniques. Researchers have exploited different physical signals such vibrations, stator current, thermal images, acoustic signals, rotor currents [8, 9, 10, 11]. Various models-based diagnostic systems exploiting different methods such as finite element method [12, 13, 14, 15], analytical methods or magnetic coupled circuits method [16, 17, 18], have been established. The most accurate motor model is based on finite element method (FEM) since it can take into account the actual geometry of the machine which may lead to more accurate electromagnetic and thermal results.

In the present work, a finite element model for analyzing the temperature distribution and the harmonic spectrum of the magnetic vector potential (MVP), is introduced in order to assess the state of operating of the induction motor. The developed model is implemented under MATLAB software and the results are obtained for the healthy and faulty operating conditions.

Electromagnetic problem formulation

The governing magnetic field equation in term of MVP is given as follows in the 2D cartesian coordinates:

$$\frac{\partial}{\partial x}\left(\upsilon\frac{\partial A}{\partial x}\right)+\frac{\partial}{\partial y}\left(\upsilon\frac{\partial A}{\partial y}\right)-j\omega g\,\sigma A=-J_S \tag{1}$$

$$\vec{J}_S=\left(kf.\frac{N_C}{S_C}I\right)\cdot\vec{n} \tag{2}$$

where, υ is the magnetic reluctivity of material and A is the MVP, σ the electrical conductivity and g the slip. J_S is the source exciting current density, N_C and S_C are respectively the number of coil turns and the cross-sectional area of the coil, $\vec{n}$ is the unit vector along the direction of the exciting current I. K_f is the volume occupation space coefficient and ω is the pulsation.

The current density of the stator winding is given by the following system:

$$\begin{cases} J_{s1}=J_{s\,max}\ \cos\omega t \\ J_{s2}=J_{s\,max}\ \cos\left(\omega t-\dfrac{2\pi}{3}\right) \\ J_{s3}=J_{s\,max}\ \cos\left(\omega t+\dfrac{2\pi}{3}\right) \end{cases} \tag{3}$$

Using the Galerkin finite element method, the expression (1) is written in space as follows:

$$\begin{aligned} &\iint_{\Omega}\upsilon\left(\frac{\partial\alpha_i}{\partial x}\frac{\partial A}{\partial x}+\frac{\partial\alpha_i}{\partial y}\frac{\partial A}{\partial y}\right)dx\,dy+\iint_{\Omega}\left(\alpha_i\ \ j\omega g\sigma A\right)dx\,dy \\ &-\int_{\Gamma}\left[\alpha_i\left(\frac{\partial A}{\partial n}\right)\right]d\Gamma=\iint_{\Omega_S}\left(\alpha_i J_S\right)dx\,dy \end{aligned} \tag{4}$$

where Γ is the boundary surrounding the meshed regions area Ω, and Ω_s is the area of the conductors. α_i represents the shape function. By the introduction of the approximation functions of the MVP eq. (4), and considering the term on the boundry Γ equal to zero, we will obtain the following algebraic system of equations:

$$([M]+ j\omega g [K])[A]=[F] \quad (5)$$

where, $[M]$ is the stiffness matrix, $[K]$ is the mass matrix, $[F]$ represents the source vector and $[A]$ is the vector of the unknown.

Thermal problem formulation

For thermal equations in the considered regions, considering Fourier's Law by applying the first thermodynamics principal in an elementary volume Ω, the equation may be given in its general form by:

$$\rho C_p \frac{\partial T}{\partial t} = div(\lambda \vec{grad}(T)) + q(T) \quad (6)$$

$$\left[-\lambda \frac{\partial T}{\partial n}\right]_{\Gamma h} = h_c[T - T_a] \quad (7)$$

where ρ is the mass density, C_p is the specific heat, λ the thermal conductivity, q is the power density, T is the unknown temperature located in (x,y) at time t and the ambient temperature is T_a.

In the same way as in the electromagnetic modelling in the Cartesian case, equation (6) is given as follow:

$$\frac{\partial}{\partial x}\left(\lambda \frac{\partial T}{\partial x}\right) + \frac{\partial}{\partial y}\left(\lambda \frac{\partial T}{\partial y}\right) - \rho C_p \frac{\partial T}{\partial t} = -q(T) \quad (8)$$

Using the Galerkin's procedure, and after shape function projection at each node of the finite element mesh, the resulting discrete form of expressions (7) and (8) is obtained as follow:

$$\iint_{\Omega} \lambda \left(\frac{\partial \alpha_i}{\partial x}\frac{\partial \alpha_j}{\partial x} + \frac{\partial \alpha_i}{\partial y}\frac{\partial \alpha_j}{\partial y}\right) dxdy\{T_i\} + \int_{\Gamma h} h_c (\alpha_i \alpha_j) d\Gamma_h \{T_i\} + \iint_{\Omega} \rho C_p \alpha_i \frac{\partial(\alpha_j T_i)}{\partial t} dxdy - \int_{\Gamma h} h_c (\alpha_i \alpha_j) d\Gamma_h \{T_a\} = \iint_{\Omega} q(T) \alpha_i dxdy \quad (9)$$

The time derivative is replaced by a finite difference. The power density generated by the Joule effect in the considered regions is given as follow [19]:

$$q(T) = \frac{J^2}{\sigma_{eq}(T)} \quad (10)$$

where J, is the induced current density and σ_{eq} is given by $\sigma_{eq} = \sigma . k_f$.

Finally, one gets:

$$\sigma_{eq}(T) = \frac{\sigma_{eq0}}{1 + \alpha(T - T_a)} \quad (11)$$

where σ_{eq0} is the material equivalent electrical conductivity at ambient temperature. α is the temperature coefficient of this material.The winding of the machine is a heterogeneous element of complex structure; it consists of enameled copper wires impregnated with resin that dissipate heat by the Joule effect. Hence, the stator winding requires careful modeling since it is one of the hottest point of the machine, thus its thermal behavior must be reproduced as precisely as possible.

Like most authors, we have compared the winding to an equivalent homogeneous medium with the average thermal conductivity of $\lambda_{eq,copper}$ [20], and we have focused on determining the values of the equivalent thermal conductivity and heat capacity. Several studies provide data on the equivalent conductivity of the winding. These data come from experimentation, from numerical integration carried out on an element area section of a slot [21], from an analytical approach [22], or from finite element modeling of an elementary pattern [23].

The slot with copper and insulation is transformed to one equivalent homogeneous medium with the average thermal conductivity of $\lambda_{eq,copper}$. The steps of the transformation are illustrated in Fig.1. which gives the actual slot with wires and the equivalent slot with the equivalent wire presenting equivalent electrical conductivity and an equivalent thermal conductivity.

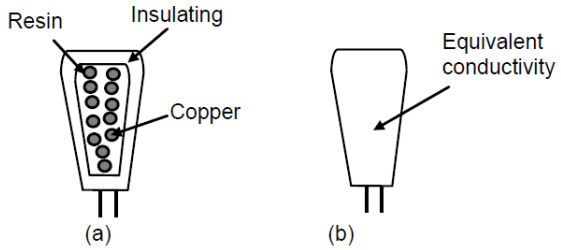

Fig.1. Transformation of the stator slot for an average thermal conductivity,(a) Original slot area, (b) Equivalent slot with an equivalent conductivity.

Conductivity of the equivalent slot is given by the following equations:

$$\lambda_{eq,copper} = \lambda_r \frac{\left(1-\sqrt{K_f}\right)\cdot \lambda_{copper} + \sqrt{K_f}\cdot \lambda_{copper}}{\lambda_r + \left(1-\sqrt{K_f}\right)\cdot \sqrt{K_f}\cdot \lambda_{copper}} \quad (12)$$

$$\lambda_{eq,copper} = \frac{\lambda_r}{1-\sqrt{K_f}} \quad (13)$$

By taking λ_r equal to 0.2 [$Wm^{-1}c^{-1}$], the thermal conductivity of a slot region is calculated as:

$$\lambda_{eq,copper} = \frac{\lambda_r}{1-\sqrt{K_f}} = \frac{0.2}{1-\sqrt{0.45}} = 0.6 \quad [Wm^{-1}c^{-1}] \quad (14)$$

The equivalent specific heat when considering two materials A and B which present respectively k_f and $(1-k_f)$ fractional ponderation volume is given by [19]:

$$\rho C_p eq = k_f (\rho_A C_{pA}) + (1-k_f)(\rho_B C_{pB}) \quad (15)$$

where the volumic mass density and the heat capacity of the materials A and B are respectively ρ_A, ρ_B and C_{pA}, C_{pB}.

Results and discussion

Fig.2 shows the geometry of the studied motor. It depicts also the considered nodes where the temperature data are calculated. The electric parameters are given by Table1, while Table2 and Table3 give respectively the geometrical and thermal characteristics of the considered motor.

Table 1. Electrical characteristics of the induction motor

Components	Value
Rated electrical power	2.2kW
Number of phase	3
Frequency	50Hz
Rated voltage	380 V
Rated current	5.2 A
Rated speed	1420 rpm

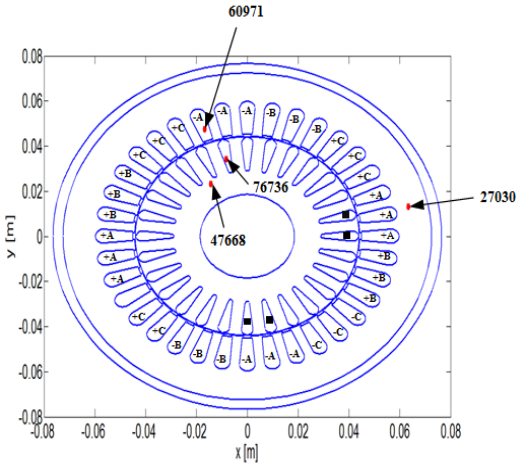

Fig.2. **C**: First Fault: Phase C open
■ : Second Fault: Four bars broken
C/ ■ : Third Fault: Phase C open and four bars broken
● **:** Nodes temperatures evaluations

Table 2. Geometrical characteristics of the induction motor

Components	value
Frame diameter	153mm
Stator outer diameter	145 mm
Stator inner diameter	88.5 mm
Number of stator slots	36
Rotor outer diameter	88mm
Rotor inner diameter	57.75mm
Shaft diameter	37mm
Number of rotor slots	28

Table 3. Thermal characteristics of the induction motor

Components	Thermal Conductivity (W/m .°C)	Heat Capacity (J/kg. K)	Mass density (Kg/m^3)
Stator	71	444	7860
Moving armature (Rotor)	51	460	7750
Copper	386	383	8954
Conductors insulator	0.2	1700	1350
Air	0.025	1600	1.2
Aluminum	204	896	2707

Healthy operating

Fig.3 (a) shows the finite element mesh of the solved domain for the electromagnetic and thermal problems. Linear first-order elements are used for the domain discretization. Fig.3(b) shows the fux lines distribution for healthy operating of the induction motor. The lines form four poles. Fig.4 gives the MVP waveforms in the air gap.

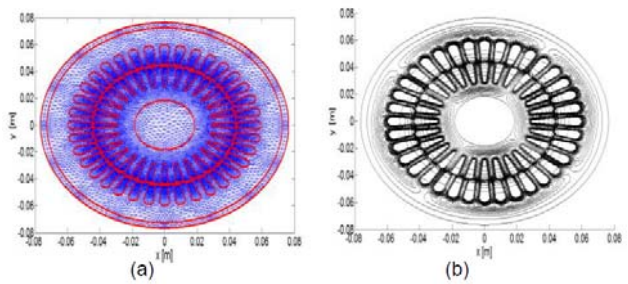

Fig.3. Finite element mesh for the electromagnetic and thermal problems (a), Flux lines distribution in the induction motor in healthy operating (b).

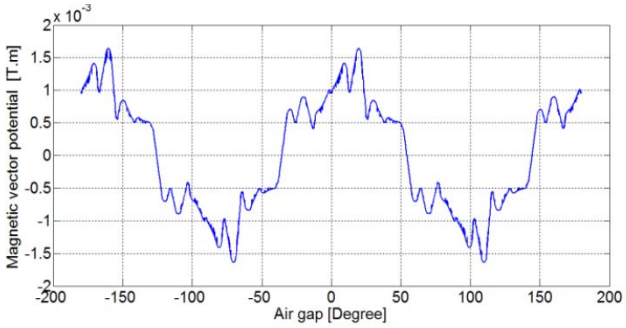

Fig.4. MVP air gap wave form in healthy operating

Figure.5 depicts the distribution of the temperature in the induction motor for the case of healthy operating.

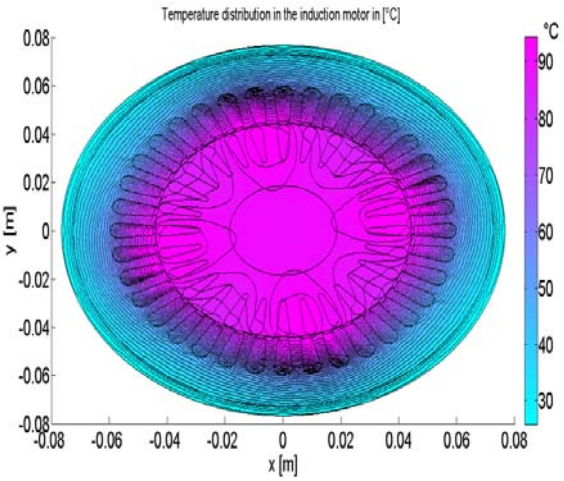

Fig.5. Isotherms in induction motor in healthy operating

Figure.6 gives the temperatures versus time at node (60971), node (76736), node (27030) and node (47668) representing different regions of the motor respectively the stator slot, the rotor bar, the stator back iron and the rotor back iron as shown in Fig.2.

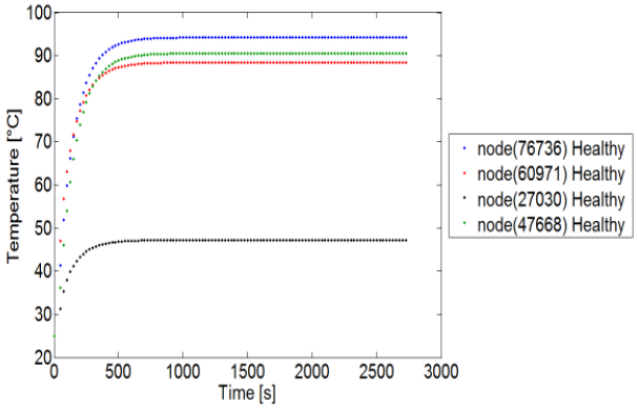

Fig.6. Temperature versus time computed at nodes representing different regions of the induction motor in healthy operating

Faulty operating with phase C open

We present the results for the case of the faulty operating of the induction motor. The first considered fault is only open circuit fault. When phase C is open, several simulations have been carried out to evaluate the effect of this type of faults on the magnetic vector potential, and on the temperature. Fig.7 and Fig.8 show respectively the

superposition of the air gap MVP wave form and the harmonic spectrum representation of MVP in faulty (Phase C open) and healthy operating conditions. As seen from Fig.8, we notice that in the healthy case the spectral representation shows the presence of several harmonics due to the non sinusoidal and noisy form of the magnetic vector potential curve. In the faulty case, we see the appearance of other harmonics and the reduction for some others, this is due to the opening of phase C compared to healthy operating state.

. .

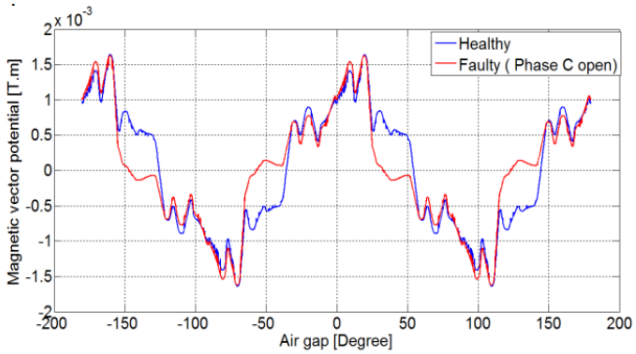

Fig.7. MVP air gap wave form in faulty (Phase C open) and healthy operating

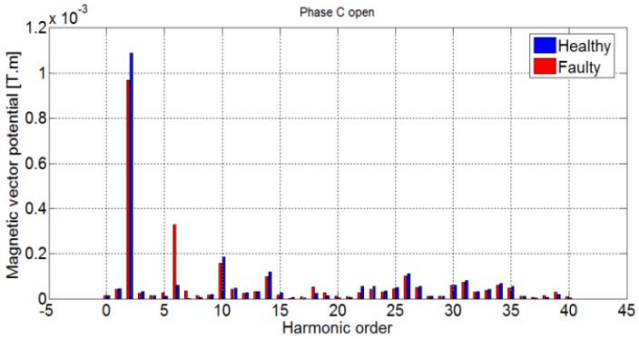

Fig.8. Harmonic spectrum representation of the MVP in faulty (Phase C open) and healthy operating

Fig.9 gives the superposition of the temperature versus time at node (60971), node (76736), node (27030) and node (47668) in healthy and faulty operating when phase C is open. As seen from Fig.10, we notice that the temperatures in the case of healthy operating are more important compared to those of faulty operating.

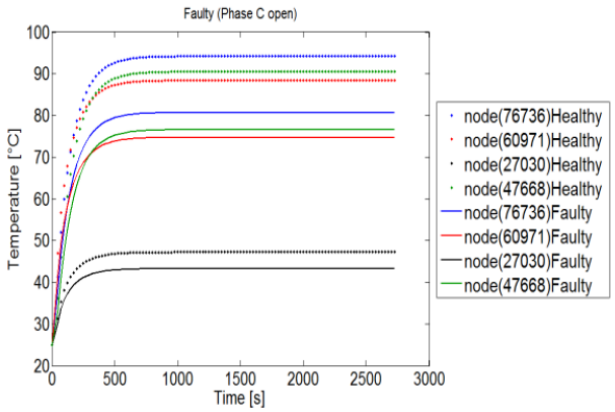

Fig.9. Temperature versus time representing different regions of the faulty motor (Phase C open) and healthy operation

Faulty operating with four broken rotor bars

The second considered fault is only broken rotor bars. We consider in this case, four broken rotor bars as shown in Fig.2. Fig.10 and Fig.11 show respectively the superposition of the air gap MVP wave form and the harmonic spectrum representation of the MVP in faulty operating with four broken rotor bars and healthy operating. Fig.11 shows that in the faulty case most harmonics situated between rank 1 and rank 25 have significantly increased due to the broken four bars of the rotor.

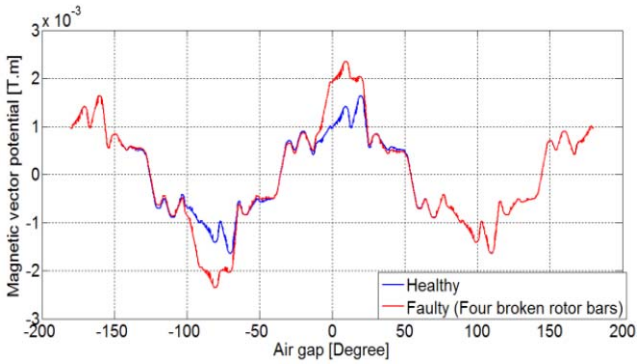

Fig.10. MVP air gap wave form in faulty (Four broken rotor bars) and healthy operating

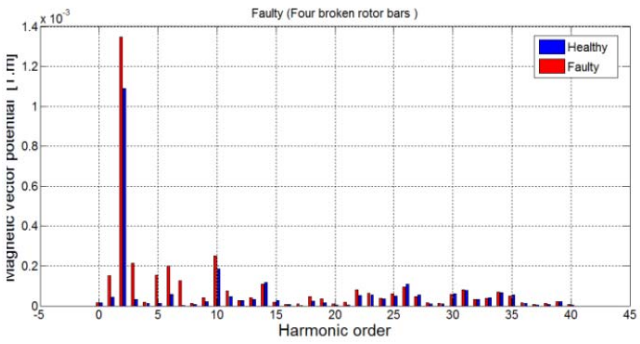

Fig.11. Harmonic spectrum representation of the MVP in faulty (Four broken rotor bars) and healthy operating

Fig.12 shows the superposition of the temperature versus time at node (60971), node (76736), node (27030) and node (47668) in healthy and faulty operating in the case of four broken rotor bars. By comparing the temperatures given in the healthy and the faulty cases, it can be noticed that the temperatures in faulty operating have significantly increased only in node (27030) compared to the tempearture in the same node in healthy operating. This increase is about 4.6 °C.

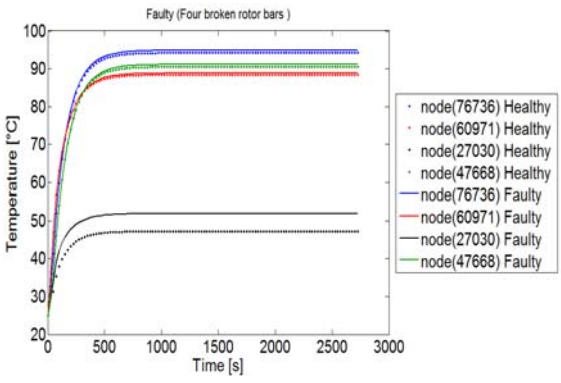

Fig.12. Temperature versus time representing different regions of the motor faulty (Four broken rotor bars) and healthy operatings

Fault operating with four broken rotor bars and phase C open

The third simulation is relative to the case of four broken rotor bars and phase C open simultaneously. Fig.13 and Fig.14 give respectively the superposition of the air gap MVP wave form and the harmonic spectrum representation of the MVP in faulty operating with four broken rotor bars and healthy operating. In Fig.14, and compared to the healthy operation, it is shown that in the faulty case, the harmonics situated between rank 1 and rank 20 have significantly increased due to the broken four bars and phase C open.

Fig.13. MVP air gap wave form in faulty (Four broken rotor bars and Phase C open) and healthy operating

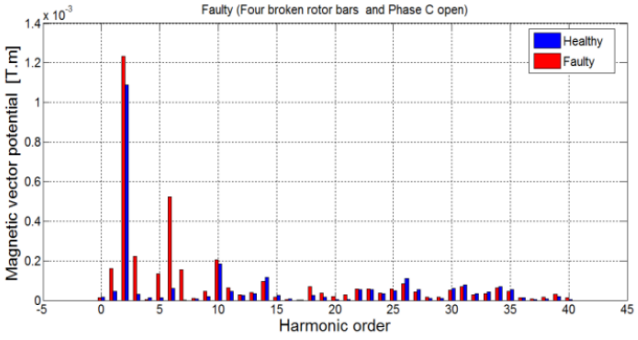

Fig.14. Harmonic spectrum representation of the MVP in faulty (Four broken rotor bars and Phase C open) and healthy operating

Fig.15 gives the superposition of the temperature versus time at node (60971), node (76736), node (27030) and node (47668) in healthy and faulty operating when four rotor bars are broken and phase C open. Fig.15 shows that the temperatures in the case of faulty operating have significantly decreased in the major considered nodes compared to those of faulty operating.

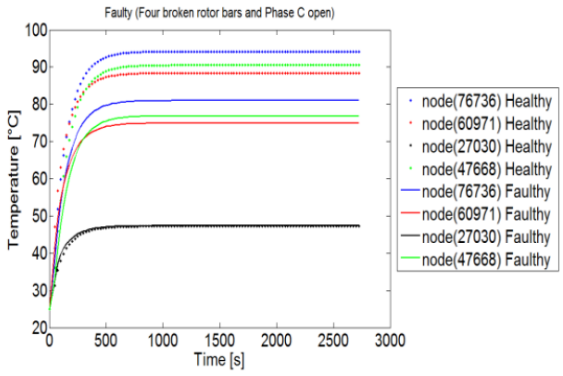

Fig.15. Temperature versus time representing different regions of the motor faulty (Four broken rotor bars and Phase C open) and healthy operatings

We can see from the results above that in the case of broken rotor bars, an increase in temperature is registered. Table 4 gives a recapitulation of the temperatures at steady state in the different considered points. The temperatures decrease in the case of stator open phase, however in the case of broken rotor bars, the temperatures increase. This shows that temperature may constitute an indication of the presence of defect in the motor. Furthermore, the flux density waveform presents perturbations in the defect zone.

Table 4. Temperatures in healthy and faulty operating

Node	Healthy	Faulty Phase C open	Faulty four broken rotor bars	Faulty four broken rotor bars and Phase C open
76736	94.205 °C	80.683 °C	94.869 °C	80.992°C
60971	88.397 °C	74.727 °C	88.827 °C	74.930°C
27030	47.219 °C	43.238 °C	51.893 °C	47.364°C
47668	90.508 °C	76.585 °C	92.029 °C	76.881°C

Conclusion

In this paper, a 2D finite element thermal modeling of three-phase squirrel cage induction motor under healthy and faulty operating conditions is presented. In this context, a electromagnetic-thermal model was solved and implemented under MATLAB software. The coupling parameter between the two models is the Joule power density.Three sorts of faults were investigated, they consist first of a stator open phase, namely phase C, the second fault consists of four broken rotor bars. the third case is four broken rotor bars and the stator phase C open, simultaneously. Temperature profiles were ploted in several points representing the different regions of the studied motor. From the obtained results, we can show that the temperature distribution and the harmonic spectrum analysis may give precious information about the presence of defects in the considered induction motor.

***Authors**: dr. Mustapha ZAOUIA, Electrical Engineering Advanced Technology Laboratory (LATAGE), Mouloud Mammeri University of Tizi-Ouzou, Algeria, E-mail: zbmust@yahoo.fr; dr. Arezki FEKIK, Akli Mohand Oulhadj University of Bouira, Algeria, E-mail: arezkitdk@yahoo.fr; dr. Abderrezak BADJI, Electrical Engineering Advanced Technology Laboratory (LATAGE), Mouloud Mammeri University of Tizi-Ouzou, Algeria, Email: badji_ummto@yahoo.com; Pr. Nacereddine BENAMROUCHE, Electrical Engineering Advanced Technology Laboratory (LATAGE), Mouloud Mammeri University of Tizi-Ouzou, Algeria, Email: benamrouchen@yahoo.com,*

REFERENCES

[1] Thorsen OV, Dalva M, A survey of faults on, induction motors offshore oil industry, petrochemical industry, gas terminals, and oil refineries, *IEEE. Trans. Ind. Appl.,* 31(1995), No.5, 1186-1196.

[2] Subrata Karmakar, Surajit Chattopadhyay, Madhuchhanda Mitra, Samarjit Sengupta, Induction Motor Fault Diagnosis,Approach through Current Signature Analysis, *Power System (2016),* ISBN 978-981-10-0623-4.

[3] Henao H, Capolino G-A, Fernandez-Cabanas M, Filippetti F, Bruzzese C, Strangas E, Pusca R, Estima J, Riera-Guasp M, Hedayati-Kia S, Trends in fault diagnosis for electrical machines: a review of diagnostic techniques. *IEEE. Ind. Elect. Mag.,* 8(2014) No.2, 31–42

[4]Anurag Choudhary, Deepam Goyal, Sudha Letha Shimi , Aparna Akula, Condition Monitoring and Fault Diagnosis of Induction Motors: A Review, *Archives of Computational Methods in Engineering* 26 (2019), 1221–1238.

[5] Mansour Ojagui, Reza Akhondi, Modeling Induction Motors Under Mixed Radial-Axial Asymmetry of The Air Gap Produced

by Oil-Whirl Fault in a Sleeve Bearing, *IEEE. Trans. Magn*.,(2018).
[6] Mina B. Abd-el-Malek, Ahmed K. Abdelsalam, Ola E. HassanNovel approach using Hilbert Transform for multiple broken rotor bars fault location detection for three phase induction motor, *ISA Transactions* 80(2018),439-457 .
[7] Mohd Sufian Othman , Mohd Zaki Nuawi , Ramizi Mohamed, Experimental Comparison of Vibration and Acoustic Emission Signal Analysis Using Kurtosis-Based Methods for Induction Motor Bearing Condition Monitoring, *Przegląd Elektrotechniczny*, 92 (2016), nr 11, 208-212.
[8] O. Guellouta,, A. Rezig, S. Touati, A. Djerdir, Elimination of broken rotor bars false indications in induction machines, *Mathematics and Computers in Simulation***,** *167(2020), 250-266*
[9] Adam Glowacz , Zygfryd Glowacz , Diagnosis of the three-phase induction motor using thermal imaging, *Infrared Physics & Technology* 81(2017), 7-16.
[10]Faiz J, Ebrahimi BM, Sharifian MBB. Different faults and their diagnosis techniques in three-phase squirrel-cage induction motors—a review*, Electromagnetics, 26(2006),543–69.*
[11] Ying X. Characteristic performance analysis of squirrel cage induction motor with broken bars, *IEEE. Trans. Magn*., 45(2009), No.2, 759-66.
[12] Weili L, Ying X, Jiafeng S, Yingli L. Finite element analysis of field distribution and characteristic performance of squirrel-cage induction motor with broken bars. IEEE. Trans. Magn. 43 (2007), No4,1537-1540.
[13] Hanafy Hassan Hanafy, Tamer Mamdouh Abdo , Amr Amin Adly, 2D finite element analysis and force calculations for induction motors with broken bars, *Ain Shams Engineering Journal, 5*(2014), 421-43.
[14] Ying Xie, Yunyang Wang, 3D temperature field analysis of the induction motors with broken bar fault, Applied Thermal Engineering, 66 (2014) 25-34.
[15] Xie Ying, Performance Evaluation and Thermal Fields Analysis of Induction Motor With Broken Rotor Bars Located at Different Relative Positions, *IEEE. Trans. Magn.,* 46 (2010), No.5,1243-1250.
[16] Andrian Ceban, Remus Pusca, and Raphaël Romary, Study of Rotor Faults in Induction Motors Using External Magnetic Field Analysis, *IEEE. Trans. Ind. Electron*., 2000; 59 (2012), No.5, 2082–2093.
[17] Qinkai Han, Zhuang Ding, Xueping Xu, Tianyang Wang, Fulei Chu, Stator current model for detecting rolling bearing faults in induction motors using magnetic equivalent circuits, *Mechanical Systems and Signal Processing*,131(2019) , 554-575.
[18] Caner Aküner , İsmail Timiz, Symmetrically broken rotor bars effect on the stator current of squirrel-cage induction motor , *Przegląd Elektrotechniczny*, 87 (2011), nr 3, 313-314.
[19]E. Chauveau, Contribution au Calcul Electromagnétique et Thermique des Machines Electriques Application à l'Etude de l'Influence des Harmoniques sur l'Echauffement des Moteurs Asynchrones, *PHD Thesis, Nantes, France* (2001).
[20] Kremers, M.F.J. ; Motoasca, T.E. ; Paulides, J.J.H. ,Transient thermal analysis of flux switching PM machines, *8th International Conference and Exhibition on Ecological Vehicles and Renewable Energies (*2013),1-7.
[21] M. Broussely, Réduction de modèles thermiques par la théorie des réseaux, application à la surveillance d'une machine asynchrone par couplage d'un modèle thermique réduit avec un schéma équivalent électrique, PHD Thesis, University of Poitiers (France), december 2000.
[22] G. S. Springer and S. W. Tsai,Thermal Conductivity of Unidirectional Materials, Journal of Composte Materials, Vol. 1, No. 2, 1967, pp. 166-173.
[23] D.T. Lussier, S.J. Ormiston, R.M. Marko, Theoretical determination of anisotropic effective thermal conductivity in transformer windings, *International Communications in Heat and Mass Transfer*, 30 (2003), No.3,311-322.